university of groningen

Metamaterial design for exoskeleton to alleviate excessive spinal load

Bachelor Integration Project

January 19, 2024

Author:
S. (Simon) Veldkamp S4460367

1st supervisor:
dr. A.O. (Anastasiia) Krushynska
2nd supervisor:
dr. ir. M. (Mozhdeh) Taheri

Word count: 7770

CONTENTS

I. ABBREVIATIONS

Computational Mechanical and Materials Engineering (CMME)
Engineering and Technology Institute Groningen (ENTEG)
University Medical Centre Groningen (UMCG)
Pain pressure threshold (PPT)
Thermoplastic Polyurethane (TPU)
Acrylonitrile Butadiene Styrene (ABS)
Polylactic Acid (PLA)
Alternating slit (AS)
Split-thickness skin grafting (STSG)

***Abstract*— This bachelor integration project researches the possibility of using mechanical metamaterials in a passive exoskeleton worn by ambulance personnel and nurses to alleviate spinal load. Currently this exoskeleton uses elastic rubber bands as shoulder straps that exert excessive load onto the spine. Mechanical metamaterial structures, in specific auxetics, are a promising solution to redistribute the load thus bringing it below the level of excessive load.**

An overview of auxetic mechanical metamaterials is presented. COMSOL simulations on the auxetics show that the honeycomb design and the alternating slit design are promising solutions for this application. This is then validated by 3D printing the design structures and tensile strength testing of these structures.

***Index Terms*— Mechanical metamaterials, passive exoskeleton, alleviate excessive spinal load, auxetics**

II. INTRODUCTION

Exoskeleton devices are currently used for people who have gait disability or reduced muscle strength due to spinal cord injury [1]. These devices help alleviate the load that is required for walking and bending. The Computational Mechanical and Materials Engineering (CMME) group at Engineering and Technology institute Groningen (ENTEG) is researching for the University Medical Centre Groningen (UMCG) which design of an exoskeleton is the most suitable for wearing during work by ambulance personnel and nurses to alleviate working load on the spine and therefore decrease the risk of lower back injuries.

The quality of healthcare is increasing each year [2]. Yet, to be able to take care of all people in need of healthcare there is high demand for healthcare workers such as nurses and ambulance personnel [3]. This high demand means the healthcare of these workers must increase also. An exoskeleton device can be used to alleviate spinal load for ambulance personnel and nurses [1]. Therefore, wearing an exoskeleton can mitigate the risk of lower back injuries while working. Thus, an exoskeleton device will improve the working conditions of medical staff. The end user of the exoskeleton discussed in this report will be the nurses and ambulance personnel of the UMCG.

A promising solution to new designs of exoskeletons can be based on mechanical metamaterials. Mechanical metamaterials are heterogeneous hybrid materials that can be designed and manipulated to obtain extraordinary properties arising from its structure and composition beyond those that a classical composite of the same material exhibits [4]. Mechanical metamaterial designs include among others Re-entrant honeycombs, Star-shaped models, Chiral models, Perforated sheet model and Rotating polygonal models [5]–[7]. Metamaterial structures can improve the mechanical properties of the exoskeleton device and ensure better load redistribution as compared to the current design. Metamaterial structures can be categorized by their mechanical behaviour.

Material selection and design is important for a passive exoskeleton aimed to decrease spinal load of its user. A passive exoskeleton is an exoskeleton that is not powered by electricity. Current passive exoskeletons at UMCG use elastic bands. These bands are located around the shoulder (see figure 1) and attached to the housing on the back. Due to the material properties of elastic bands, excessive compression force is imposed on the vertebrae. In this report, the proposal for a best suited metamaterial

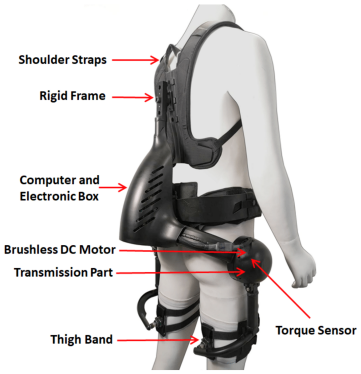

Fig. 1: Example of exoskeleton, used to alleviate spinal load [8].

structure design will be made. A metamaterial design of the shoulder straps will be thoroughly examined in terms of their mechanical characteristics and performance. The metamaterial design must preserve the functionality of the exoskeleton shoulder straps.

The structure of this report will be as follows. After the introduction, the conceptual design with a problem analysis, system description, Why-What analysis, Stakeholder analysis, problem statement, research objective, research framework and research questions will be presented. Thereafter, the technical research design will be stated, consisting of methods and tools, research planning and deliverable and validation. Following this, an overview of mechanical metamaterials and auxetic design structures will be provided. Then initial manufacturing and tensile testing followed by COMSOL simulations for design optimization and tensile strength testing will be explained. At last, a comparison between the COMSOL simulations and tensile testing results will be made followed by the conclusion and discussion.

III. CONCEPTUAL DESIGN

A. *Problem context*

An exoskeleton is a device which is strapped onto the body of the user and is used to reduce the stress acted upon the body parts. In this study the focus is on an exoskeleton which is strapped onto the back of the user that reduces the spinal load of the user while performing tasks. In figure 1, an example of a general active exoskeleton is provided. The exoskeleton that is relevant for this study is classified as a passive exoskeleton. This exoskeleton shares identical

components (as figure 1), except for the torque sensor, transmission part, brushless DC motor and the computer and electronic box which are missing in the passive design.

The current material proposed for the shoulder straps in the development of a passive exoskeleton used to alleviate spinal load is elastic rubber bands. Rubber has a high Poisson ratio (close to 0.5) that describes the material contraction in the direction opposite to that of an applied force under tension. The Poisson's ratio shows the amount of displacement a material demonstrates in directions that are normal to the force acted upon the material and is given by formula 1[9].

$$v = -\frac{e_{trans}}{e_{axial}} \tag{1}$$

where e_{trans} is the strain in the transverse direction and e_{axial} is the strain in the axial direction.

A material that has a high Poisson's ratio means that the area becomes rapidly compressed when the material get stretched. Thus, greater stress is exerted when stretching of the materials occurs [9]. This behaviour is explained by the fact that stress is defined as the following.

$$\sigma = \frac{F}{A} \tag{2}$$

This excessive force exerted by the elastic shoulder straps is acted upon the shoulders and thus spine of the user of the exoskeleton. The proposed new metamaterial structure design as shoulder straps should, therefore, demonstrate a low or negative Poisson's ratio. This behaviour means that during extension of the proposed metamaterial design, the area of this design will have more width and therefore reduce the stress imposed on user's shoulder. A material that exhibits a negative Poisson's ratio is also referred as an auxetic material [5]. These auxetics demonstrate counter-intuitive behaviour by expanding in width under tension and contracting under compression. This auxetic behaviour is compared to that of materials with a positive and zero Poisson's ratio in figure 2.

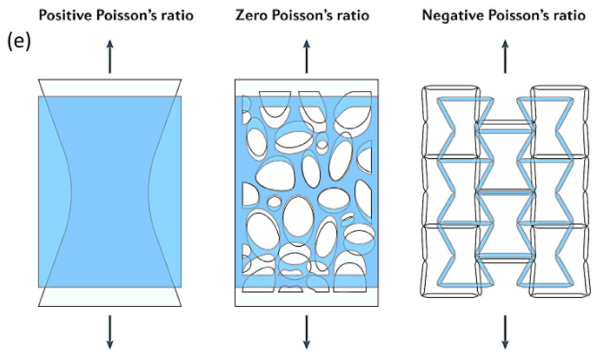

Fig. 2: Comparison of structures with positive, zero and negative Poisson's ratio [10].

There are three examples displayed in figure 3 of metamaterial structures. These examples have different configurations of the unit cells, as well as different thickness.

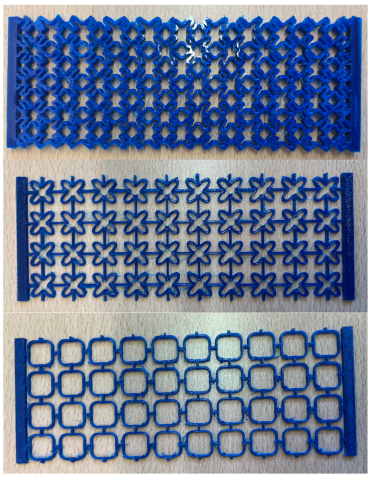

Fig. 3: Three different examples of metamaterial structures.

The problem owner is dr. Anastasiia Krushynska, as she is leading this research at the CMME group at ENTEG. She is the one that is supervising this project and took on the problem at hand.

Functionality: The new proposed metamaterial structure design must maintain the functionality the current design already has while decreasing the excessive spinal load on the user. The functionality of the exoskeleton can be measured by the following parameters.

1) First, the design should **work properly**. The new design should be able to be at least just as if not less prone to failure. The design should be able to withstand the forces acted upon itself by the generated displacement.
2) Comfortability; Secondly, the newly proposed design should be **comfortable** for the user. It should be convenient for the user to wear the exoskeleton. The comfortability can be measured by pain pressure threshold (PPT) value [11]. However, for this research, only the material characteristics are taken into account since pressure sensors would be needed to determine if the pressure would not exceed the PPT value.
3) Spinal load; Third, the **spinal load** of the new design structure should be less than the current design. This load can be measured by the compression forces the new design exerts on the user which is determined by the Poisson's ratio and contact area of the design. This means that the Poisson's ratio should be smaller than the current design, while the contact area should be maximized.

For this project there are three different materials to be chosen from. The only materials that are available at the RUG and comply within the boundaries of this system are

Thermoplastic Polyurethane (TPU), Acrylonitrile Butadiene Styrene (ABS) or Polylactic Acid (PLA). There are three different TPU's available at the RUG. These are Kimya, Prosthetic and VarioShore TPU.

B. *System description*

The scope of this project is limited to the shoulder straps of the exoskeleton. Active exoskeletons are not within the scope of this project, due to the fact that the UMCG is designing a passive exoskeleton. For this project, only 3D printing facilities will be used to manufacture the design. Although there are also other manufacturing methods available at the RUG, this is a good already proven method to get desired results and ultimately propose a good recommendation for a new design. This project also only considers the structural manipulation of materials, since the metamaterial design will only consist of one material. The system is visualised in figure 24 in the appendix.

C. *Problem analysis*

1) Why-What analysis: A Why-What analysis is formed following the principles of N. Annamalai [12] and can be seen in figure 4.

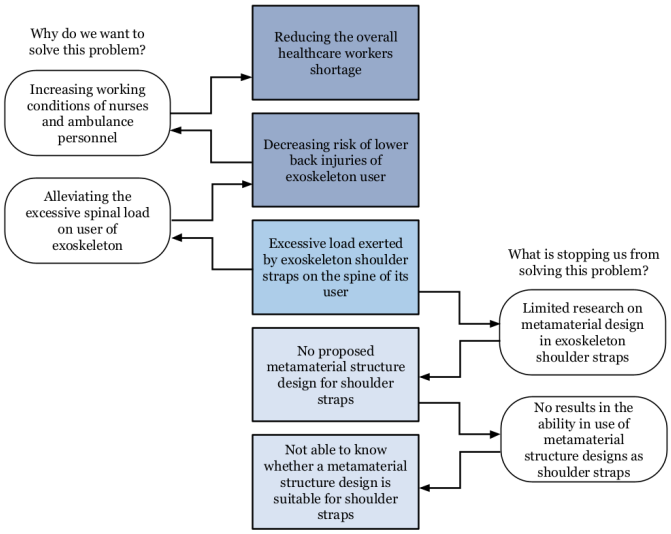

Fig. 4: Why-what analysis following the principles of [12].

2) Stakeholder analysis: The following stakeholders are defined: UMCG, RUG, dr. Anastasiia Krushynska at CMME and Nurses and ambulance personnel.

Dr. Anastasiia Krushynska at CMME is a stakeholder with a high interest since she is the problem owner, which means that she has high power and high interest.

The **nurses and ambulance personnel** have high interest in this research, since they will be the final users of the metamaterial structure design of the exoskeleton.

The **RUG** needs to keep satisfied; they have relatively high power but relatively low interest. Since dr. Anastasiia Krushynska is taking on this project as problem owner, RUG has relatively high power. This stakeholder has some interest in this project, but significantly less than dr. Anastasiia Krushynska and the end users of the exoskeleton.

UMCG is a stakeholder that has relatively low interest and power. This stakeholder needs to be monitored and is not directly involved within this research.

The stakeholder analysis is displayed in figure 5. This stakeholder analysis is done following the principles of Ackermann and Eden [13].

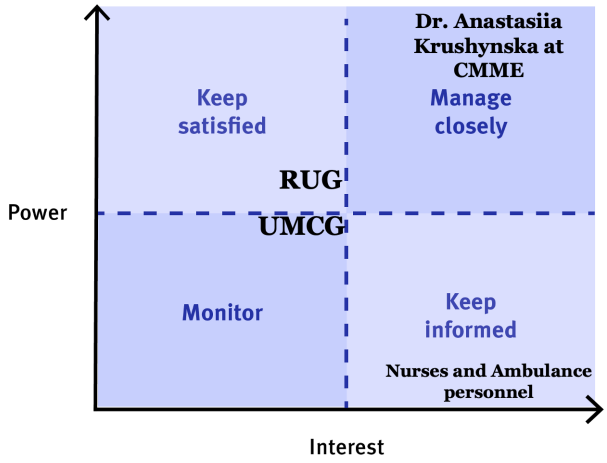

Fig. 5: Stakeholder analysis following Ackermann and Eden [13].

D. *Problem statement*

The problem statement is derived from the problem analysis and problem context. The problem statement is defined as the following. The elastic rubber bands as shoulder straps of the exoskeleton of whose purpose has to reduce the risk of lower back injuries, exert excessive compression force on the spine in both neutral and flexed position.

E. *Research objective*

The research objective is to find, evaluate, 3D print and test the best suited metamaterial structure design that can replace the current elastic band design of the exoskeleton's shoulder straps in order to decrease excessive loading on the shoulders and thus spine, while preserving the functionality of the current exoskeleton design.

This objective must be obtained in a time span of 10 weeks starting the 6th of November, meaning that the deadline is 19th of January.

A meaningful research objective should be **Smart**, meaning specific, measurable, attainable, relevant and time-bound [14]. **Specific**: a clear end goal is envisioned in the form of 3D printed metamaterial samples. **Measurable**: because the mechanical properties of the produced samples can be estimated in simulations and tensile testing. **Attainable**: within the given time period the objective is attainable, as

can be seen in the research planning (fig. 26). The objective is **relevant**, as ambulance personnel and nurses have a high risk at lower back injuries. Excessive load imposed on the spine also causes a higher risk of lower back injuries. **Time-bound**: a clear time span is given namely 10 weeks with a hard deadline on 19th of January.

F. *Research framework*

First, extensive literature research needs to be conducted regarding different metamaterial structure designs. Concurrently, initial designs structures will be subjected to simulation to acquire a more comprehensive understanding of their behaviour under tensile force. Based on the findings from the literature research and initial design simulations, several different designs are identified to be suited as a new design structure for the shoulder straps of the exoskeleton. The design structures will be subjected to tensile force in COMSOL simulations, since that is the only significant force they will undergo.

After initial 3D printing and tensile testing of the best suited designs, the best suited design structure will be chosen and this design will be simulated under different parameters. The parameters of a metamaterial design that will be studied are unit cell size and unit cell shape, wall-thickness and sample (structural) thickness. Finally, the best suited design will be 3D printed and tested using a tensile strength machine to validate the simulation results and conclude on the best suited design.

The research framework is displayed in the appendix in figure 25.

G. *Research questions*

Main research question The main research question is which metamaterial design is best suited to alleviate the excessive spinal load exerted by the elastic band of the current design of the exoskeleton and what is the influence of its parameters on the deformation behaviour?

Sub questions

- Which metamaterial designs are auxetics and therefore suitable to alleviate excessive spinal loading?
- What is the behaviour of the possible suited metamaterial design under tensile strength simulation in COMSOL?
- Which is the best suited metamaterial design according to the simulations in COMSOL and preliminary 3D printing and tensile testing?
- What behaviour does the best suited metamaterial design show under tensile load in experimental stage?
- What is the influence of the parameters of the best suited metamaterial design on the deformation behaviour under tensile strength?

IV. TECHNICAL RESEARCH DESIGN

A. *Methods and tools*

The methods and tools that will be used in solving the research questions are explained in this section.

1) Methods: The first sub question is answered by **literature research**.

The second sub question will be answered by **simulating** the possible structure designs in COMSOL. The simulations will show the deformation behaviour of a certain design when a tensile force is applied.

The third sub question will be answered by the **simulation** results in COMSOL. The structure design that is best suited following the simulations in COMSOL is selected. This structure design is then 3D printed.

The final sub question will be answered by performing tensile force **experiments** in a tensile machine. The results of this test will be described in a graph. Afterwards, a conclusion can be drawn regarding the best suited metamaterial structure design that is most suitable for replacing the elastic band in the shoulder straps used in the current design.

2) Tools: For this research, multiple software will be used. The first software is **COMSOL**, used to sketch the design and thereafter perform finite element analysis. This software allows for structural mechanics simulations on the metamaterial structure. Afterwards, the best suited structure design following the structural mechanics simulation in COMSOL will be manufactured with the help of **Cura**. Cura is the software that calculates the best order to print the design. The design is uploaded to Cura, after which the design is 3D printed.

B. *Research planning*

A Gantt chart is displayed in the appendix in figure 26. This chart visualises the research planning.

C. *Deliverable and validation*

1) Deliverable: The deliverable of this research project is a proposal of a best suited design of a metamaterial structure that replaces the current elastic band of the exoskeleton's shoulder straps. This metamaterial structure must reduce compression force on the shoulders, thereby alleviate the excessive spinal load imposed on the user.

2) Validation: To validate the simulations that are made in COMSOL, the best suited structure design will be 3D printed. Afterwards, the 3D printed artefact will be tested under tensile loading in a tensile strength machine. Then results will be compared to the simulations conducted in COMSOL. If the actual testing results corresponds with the simulations in COMSOL, the 3D printed metamaterial structure design is validated.

V. MATERIAL SELECTION

TPU filament is chosen as the material to 3D print. TPU is more flexible than ABS and PLA. Flexibility in the 3D printed structure is of high importance for this project, since

the auxetic behaviour of the design structures needs to be examined. If the design structure is not able to easily strain it is more difficult to obtain the deformation behaviour.

COMSOL simulation shows that for a 10% strain, the force needed for TPU, PLA and ABS are 130.57N, 190.27N and 153.14 N respectively for the same structure. Therefore, TPU is chosen to manufacture the metamaterial design structures.

VI. MECHANICAL METAMATERIAL OVERVIEW

Mechanical metamaterials are categorised by their extraordinary characteristics arising from its structure and composition. The following categories have been proposed by A. A. Zadpoor: Extremal materials, Negative metamaterials, Ultra-property metamaterials and Emerging area [15].

A. Extremal materials

Extremal materials are defined as materials that are extremely stiff in certain modes of deformation, while extremely compliant in other modes. This concept was first introduced by Milton and Cherkaev in 1995 [16]. The eigenvalues of the elasticity tensor of the extremal material determines this behaviour. Very small eigenvalues yield a high compliance when subjected to deformation in the direction corresponding to that eigenvalue. Extremal materials can be divided into sub-sections assigned by the amount of very small eigenvalues of the elasticity tensor of the material [15].

1) Penta-mode metamaterials: Penta-mode metamaterials are extremely compliant in five out of six principal directions. This translated to a very large bulk deformation compared to their shear modulus. This yields that the volume of penta-mode metamaterials does not change as a result of deformation, which is the same as saying that the Poisson's ratio is 0.5 [17].

2) Dilational and auxetic metamaterials: The relationship between the Shear modulus (G), Bulk deformation (B) and Poisson's ratios (v) is shown in equation 3 [18].

$$\frac{B}{G} = \frac{v+1}{3(\frac{1}{2}-v)} \tag{3}$$

A dilational metamaterial exhibits an extremely small bulk deformation as compared to its shear modulus, meaning the Poisson's ratio is -1. All materials which have a negative Poisson's ratio are auxetics, thus these dilational metamaterials are also auxetics [5].

B. Negative metamaterials

Negative metamaterials exhibit negative moduli such as negative bulk modulus or negative elastic modulus. Among these negative metamaterials are negative compressibility and negative stiffness metamaterials, but also negative thermal expansion [15]. The latter is however not discussed since this research is focuses solely on mechanical behaviour of metamaterials.

C. Ultra-property metamaterials

Ultra-property metamaterials are metamaterials that posses simultaneously two or more properties that due to their conflicting nature would not be exhibited in ordinary materials. Such conflicting characteristics are for example high strength and toughness. Nature shows us however that it is possible. Nacre can for example achieve high stiffness, high toughness and high strength at the same time. This causes for researchers to develop metamaterials with rationally designed architectures that exhibit ultra-stiff, ultra-strong, ultra-tough and ultra-light metamaterials [19], [20].

D. Emerging area

Origami/ Kirigami metamaterials rely on the principles of folding and assembling typically 2D structures into intricate 3D structures. This means that the topological configuration of Origami/ Kirigami can be altered. This technique would induce metamaterials to have desirable mechanical properties, such as multi-stability, ultra-large deformation, programmable stiffness, static morphing and negative Poisson's ratio [10].

VII. AUXETICS DESIGN STRUCTURES

For this project only metamaterials with a negative Poisson's ratio (auxetics) are of importance. In this section several auxetic metamaterial design structures will be highlighted an analysed on their potential in the application to the design of the exoskeleton. The auxetic design structures are categorized by four sub categories. These sub categories are re-entrant structures, rotating rigid geometries structures, chiral structures and other structures [21]. Figure 6 visualises the re-entrant structures, rotating rigid geometries structures and chiral structures.

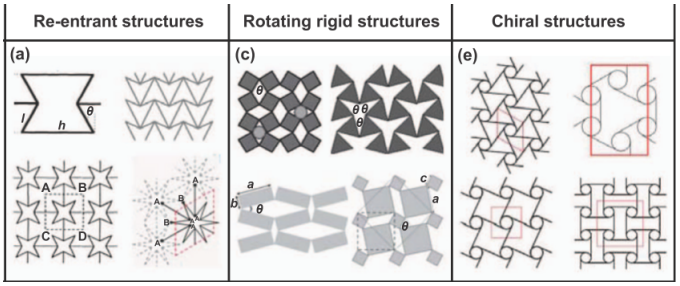

Fig. 6: Examples of re-entrant structures, rotating rigid geometries and chiral structures. Adopted from Li, Xiang [21].

Each design consists of a unit cell that is copied and multiplied six times in the horizontal direction and ten times in the vertical direction. In this project, the deformation behaviour is measured in relative values as opposed to absolute values. Therefore, the dimensions are not shown in the results of these COMSOL simulations. However, it is imperative to set the same relative strain, scale of deformation and element mesh on each design to compare the deformation behaviours. The strain applied to each

structure design is uniform at set to be 10%. The scale at which the deformation behaviour is shown is 1. The mesh is physics-controlled and has a normal element size.

The 10% strain is obtained by fixing the bottom of each structure and setting a prescribed displacement of 10% structure to the top side (y-direction). This means that the metamaterial structures are under geometric nonlinear deformation behaviour regimes, due to the large strain applied. The definition of the applied solid mechanics to a model in COMSOL is shown in figure 7.

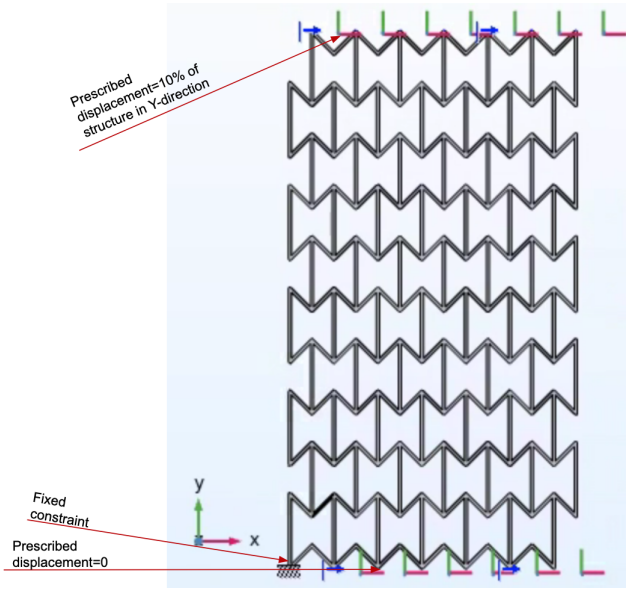

Fig. 7: Definition of the solid mechanics of re-entrant honeycomb structure as example.

Point evaluation is performed on the fifth unit cell row of the models, where the displacement in the x direction is obtained. The Poisson's ratio is then calculated using formula 1.

A. *Re-entrant structures*

1) Re-entrant honeycombs: Re-entrant honeycombs design are based on honeycomb structure. Honeycomb structures are excellent in their energy absorption capacity [22]. Honeycomb structures in nature are hexagons placed on top of each other with each side being connected to another unique hexagon, see figure 8.

The principles of this natural honeycomb structure are applied to the re-entrant honeycombs design. This structure is constructed using a unit cell of two individual hexagons that are placed on top of each other. This unit cell is thereafter copied in the horizontal axis and in the vertical axis to form the structure. The structure is displayed in figure 9.

A close up of the structure can be seen in figure 28 in the appendix. As figure 28 shows, the size of each

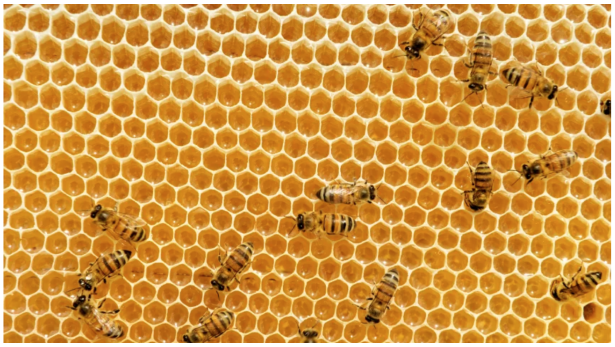

Fig. 8: Natural honeycomb structure [23].

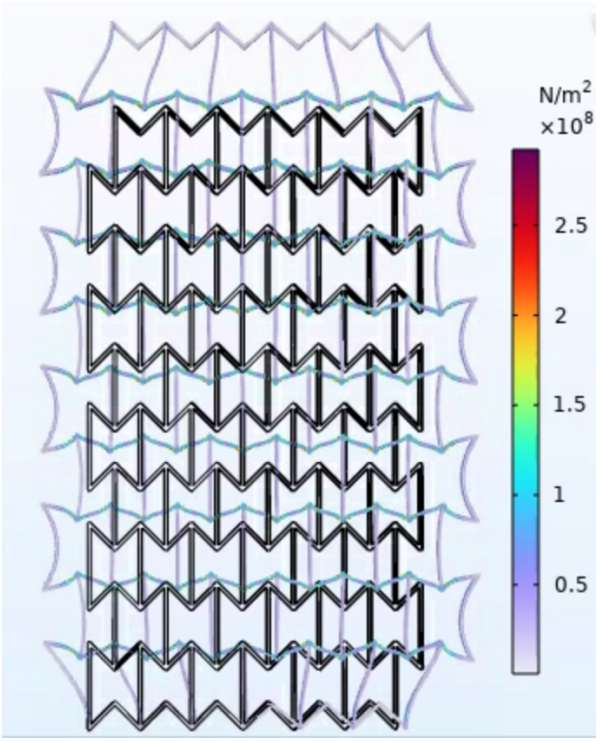

Fig. 9: Re-entrant honeycomb structure and its deformation behaviour, with the von Mises stress (N/m^2) also shown.

side of the hexagons are not equal. As a result, the angle each side makes with another side is also not uniform. This structure is highly auxetic due to the angle (θ) of the outside sides with the sides that go inward relatively small. The lower the θ the lower the Poisson's ratio and thus 'more' auxetic. It is essential to consider that the stability of this structure is also dependent on this θ.

The measured displacement on the fifth unit cell row in transversal direction is -10.317mm and 12.00mm, so the total transversal strain is 22.32mm. The axial strain is 20mm. The Poisson's ratio of the structure is

$$v = -\frac{22.32}{20} = -1.12 \tag{4}$$

2) Re-entrant star shaped: Re-entrant star shaped design structures consist of star shaped unit cells. In figure 10 a star

shaped structure is displayed which has four points. There are also other star shaped design structures such as three pointed, six pointed and one pointed shapes. The magnitude of the auxetic behaviour of this structure is defined by the angle θ each of the four points. The lower the angle, the lower the Poisson's ratio in theory. However, further simulations (figure 27a and 27b in appendix) show that by decreasing or increasing the angle θ the deformation behaviour does not significantly change. This is due to the fact that the connections between the stars are fixed horizontally and the design can therefore not deform freely in the horizontal directions.

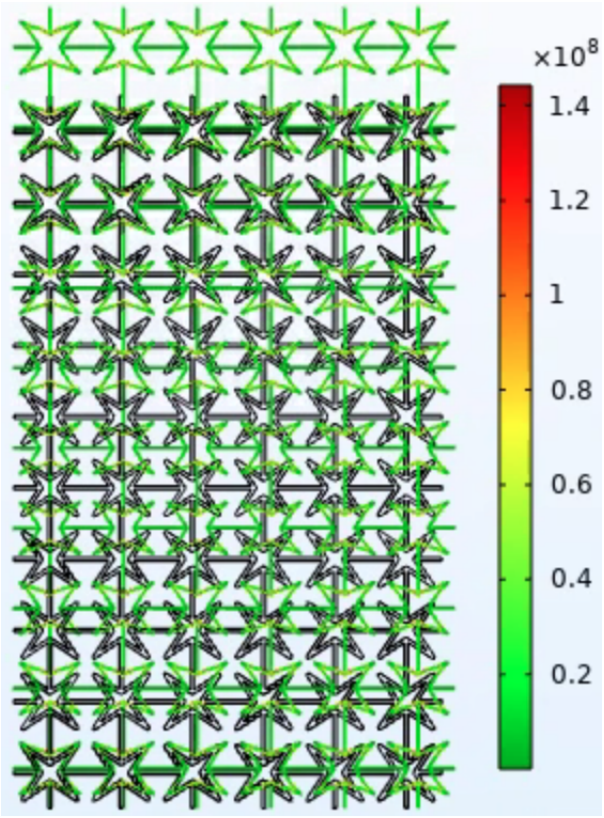

Fig. 10: Re-entrant star shaped structure and its deformation behaviour, with the von Mises stress (N/m^2) also shown.

The displacement of the fifth unit cell row in transversal direction is -2.5963mm and 3.209mm, so the total transversal strain is 5.80mm. The axial strain is 20mm. The Poisson's ratio of the structure is

$$v = -\frac{5.80}{20} = -0.29 \tag{5}$$

While this design exhibits exceptional stability and evenly distributes stress throughout the entire structure, the deformation falls short due to the Poisson's ratio being close to zero. furthermore, the contact area of this design structure is low. Therefore this structure is not suited for the application in this project.

See figure 30 in the appendix for a closeup of the structure and the stresses acted upon it.

B. Rotating rigid geometries structures

Rotating geometries structures are structures with geometries like triangles, squares or rectangles that can rotate. The assumption is made that the geometries are non-deformable along loading directions. These geometries are attached to one another on only their corners, so that they are free to rotate [5]. This concept is visualised in figure 11.

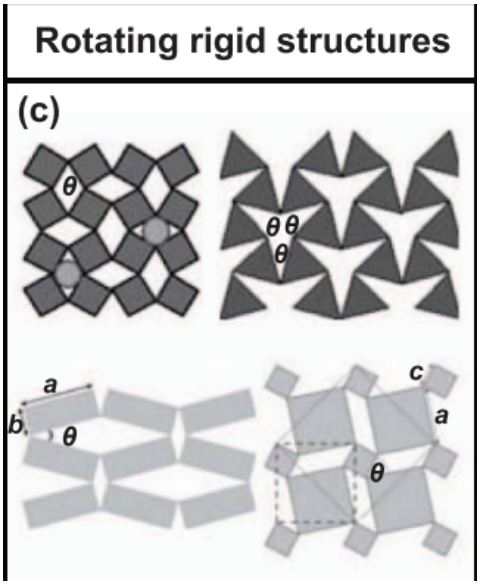

Fig. 11: Rotating ridged geometries adopted from Li, Xiang [21]. Top left; rotating squares. Top right; rotating triangles. Bottom left; rotating rectangles. Bottom right; rotating squares with different block sizes.

In this report the chosen geometry for this auxetic design structure are squares. The rotating square structure is constructed using larger and smaller blocks, these blocks can be seen in figure 29 in the appendix. The whole structure is displayed in figure 12. This design is able to rotate due to the smaller blocks which are connected to the sides of the corner of the larger blocks. The rotation of the squares cause for expansion horizontally while load is applied in the vertical direction and thus auxetic behaviour is observed.

The measured displacement on the fifth unit cell row in transversal direction is -2.81244mm and 10.772mm, so the total transversal strain is 13.58mm. The axial strain is 20mm. The Poisson's ratio of this structure is

$$v = -\frac{13.58}{20} = -0.70 \tag{6}$$

This design structure is suitable for the application of this project. However, the rotation of the squares is large which causes friction with the shoulders of the end users and ultimately can cause discomfort [24].

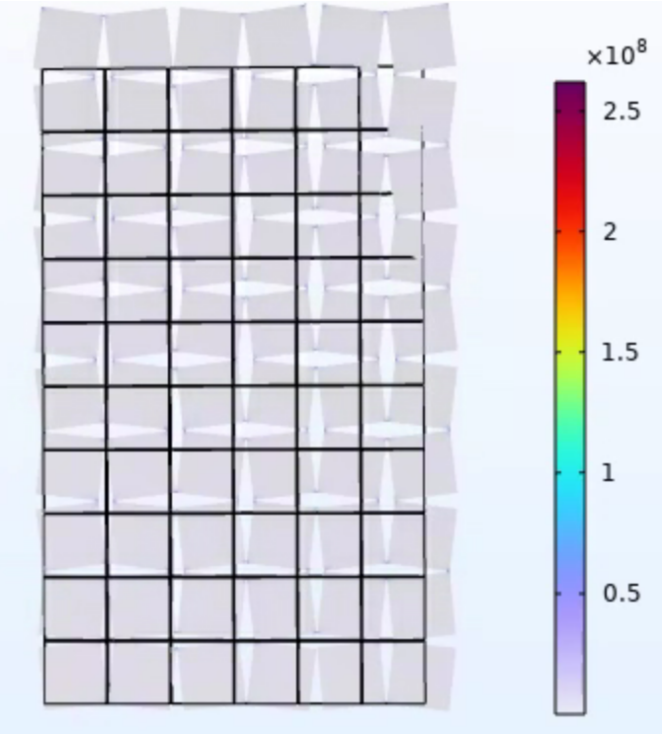

Fig. 12: Rotating square structure and its deformation behaviour, with the von Mises stress (N/m^2) also shown.

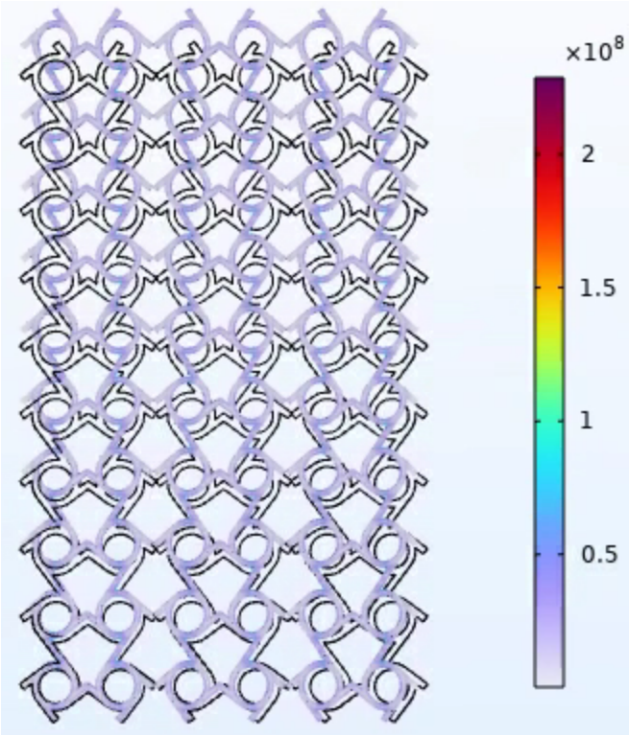

Fig. 13: Chiral structure with mirrored unit cell and its deformation behaviour, with the von Mises stress (N/m^2) also shown.

C. Chiral structures

The chiral design structure is based on chiral structures with in this case four ligaments. Chirality is a property a structure has that stands for asymmetry. This term however is often used to present a physical property of spinning [5]. This design structure can impose a negative Poisson's ratio due to the rotational ability of such chiral structures.

The deformation behaviour under tensile loading of the chiral model structure is shown in figure 14. The deformation behaviour of this design structure does not show clear auxetic behaviour. This structure does not uniformly deform vertically, but also displaces simultaneously to the right. This arises from the non-superimposable nature of the unit cell on its mirror image, leading to an overall asymmetric structure. The Poisson's ratio of the structure can therefore not be determined straightforwardly.

To solve this problem the unit cell is mirrored. The new unit cell consists of the chiral structure and its mirror image next to each other. This unit cell is placed in an array of 3 horizontally and 5 vertically to obtain the same structure size. This newly formed structure is now symmetric and its behaviour is shown in figure 13. The deformation now is symmetric, as opposed to the other chiral structure. However, what can be seen is that this structure does not show auxetic behaviour. The measured displacement in transversal direction of the fifth unit cell row is 0.164272mm and -5.2144mm, so the total transversal displacement is -5.05mm. The total axial displacement is 5mm. The Poisson's ratio of this structure is

$$v = -\frac{-5.05}{20} = 0.25 \tag{7}$$

This structure design is not auxetic and therefore not suitable for the application in this project.

Figure 31 in appendix shows a closeup of the structure and the von Mises stresses acted upon the structure.

D. Other structures

1) alternating slit: The alternating slit (AS) model is characterised by the alternating slit which are located in a larger square. Two AS models are studied upon, namely AS model where the alternating slits are in each column of the whole structure (figure 15) and an AS model where the alternating slits are in every other column (figure 16). A comparable design technique is medically used in treating skin burns and is called split-thickness skin grafting (STSG). In STSG parallel slits will be inserted in healthy skin for expansion to cover a larger burn area [25]. The AS model consists of parallel slits vertically and horizontally, with no intersections between the horizontal and vertical slits.

In figure 16 the deformation behaviour when subjected to tensile strength is shown.In addition to the structures itself a close up of the AS designs are displayed (figure 32 and 33) to get a better understanding of the structures and to show the most fragile points of the structures.

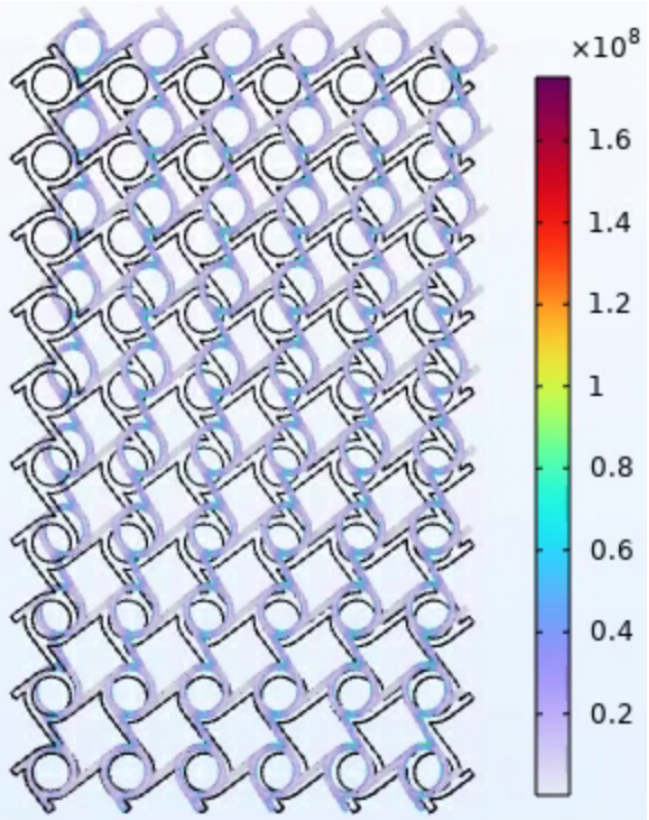

Fig. 14: Chiral structure and its deformation behaviour, with the von Mises stress (N/m^2) also shown.

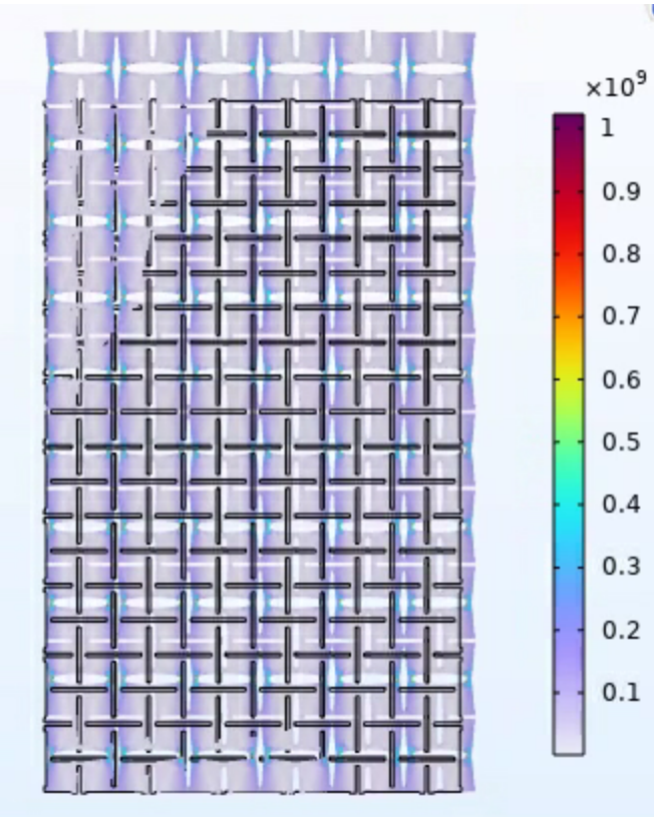

Fig. 15: AS model with AS every column and its deformation behaviour, with the von Mises stress (N/m^2) also shown.

The measured displacement of the fifth unit cell row of the AS model with every other column an alternating slit in transversal direction is 0.12403mm and 4.1039mm. This means that the total transversal displacement is equal to 3.98mm. The total axial displacement is 20mm. The Poisson's ratio of this structure is

$$v = -\frac{3.98}{20} = -0.20 \tag{8}$$

The measured displacement for the fifth unit cell row of the AS model with every column alternating slit in transversal direction is 0.12311mm and 4.1037mm. The total transversal displacement is then equal to 3.98mm. The total axial displacement is 20mm. The Poisson's ratio of this structure is

$$v = -\frac{3.98}{20} = -0.20 \tag{9}$$

This design is also suitable for the application of this project, the principles are more or less the same a the rotating squares model. The main difference is that the slits are not stretched to the end of each unit cell, causing for more area attached to each other compared to the rotating square design. This AS design has better distributed contact area and rotates less, which ultimately means that it would be more comfortable to wear.

The simulations and computations of the Poisson's ratio of the two different AS models show that they are both indifferent to each other. From now on the AS model with alternating slits each column is referred to by the AS model. This model is chosen over the AS model with alternating slits every other column due to the symmetry and controlled deformation behaviour throughout the structure.

E. Best suited metamaterial design structures

The best suited metamaterial design structures following the analysis of the auxetic design structures mentioned previously are: the re-entrant honeycomb and the AS design. The behaviour of the re-entrant honeycomb design shows auxetic behaviour of a high magnitude. The behaviour of the AS is auxetic and has a high contact area and the deformation behaviour is controlled. Furthermore, these structures show the most potential in the application of replacing the shoulder straps of the exoskeleton design.

VIII. INITIAL MANUFACTURING AND TESTING

3D printing is the manufacturing process used for this project to show the deformation behaviour of different metamaterial structures. However, some other manufacturing processes can also be used to form the shoulder strap, such as laser cutting.

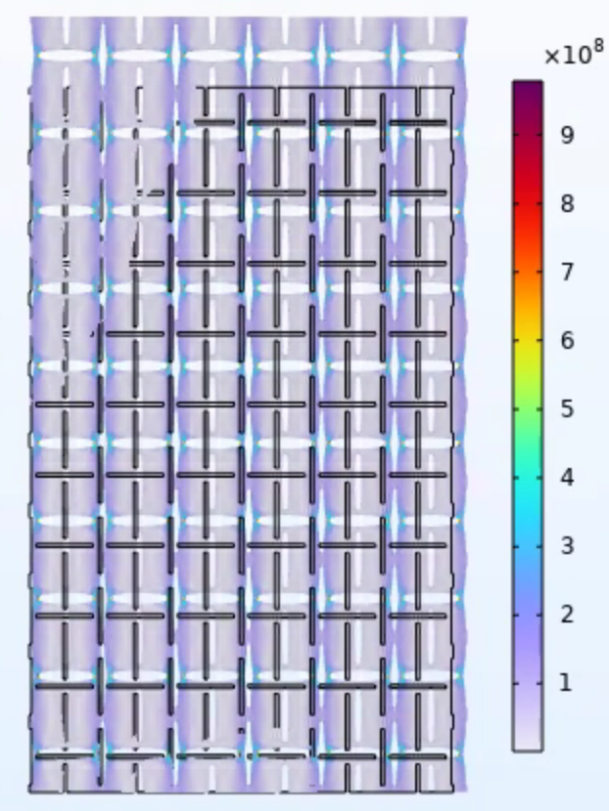

Fig. 16: AS model with AS every other column and its deformation behaviour, with the von Mises stress (N/m^2) also shown.

Laser cutting is a technique where a focused laser beam is directed onto the material that either vaporizes, burns or melts or is blown away. This technique produces sharp and precise cuts and is also possible to make sharp angles and turns [26]. Laser cutting works extraordinary good on thin sheets of material, which makes this manufacturing technique applicable for this project. This technique could have an edge over 3D printing since it is more precise that 3D printing. However, not all design structures are efficient to create using this technique. Only designs which have small or no spacing between or in its unit cells can be manufactured effectively with laser cutting. This laser cutting technique is applied to the AS design. The results show indeed that this technique can be used for this design specifically. The artefact is displayed in figure 34 in the appendix. This figure also shows the buckling effect which is further elaborated on later in this section.

The honeycomb design and the AS design are fabricated using Ultimaker 3. The printer settings that were used to get good quality prints are 240 degrees Celsius for the nozzle, 60 degrees Celsius for the bed temperature, infill of 100% and a flow speed of 20mm/s. The thickness of the sheet is 0.5mm.

The honeycomb design when subjected to tensile strength showed high auxetic behaviour. However, the honeycombs turn out of the plane (see figure 36 in appendix). This is called the buckling effect. This mode occurs due to a bending moment that is being generated by shear stress acted upon the structure [27]. Furthermore, although this design shows extremely high auxetic behaviour, the contact area of this design would be especially small compared to the alternating slit design. The contact area can be improved by scaling the unit cells down, however for this project this is not feasible, due to limitations of the applied manufacturing process. The unit cells must be scaled down by at least a factor of 10 to come even remotely close to the contact area the AS design offers. The 3D printer is not able to print such small unit cells, since the nozzle is too big.

The alternating slit design shows significantly lower auxetic behaviour. The deformation behaviour is still auxetic and conform the requirements of the new design. The contact area of this design is extraordinary large. The only part of the design which does not have contact with the shoulder of the user are the slits. This means that the load distribution throughout the design on the shoulder is excellent. The deformation of each unit cell is relatively low, hence the relatively high Poisson's ratio compared to the honeycomb design. This ultimately means that this design structure is stable overall and best suitable for the application of this project.

IX. COMSOL SIMULATIONS FOR DESIGN OPTIMIZATION

In this section the best suited design will be subjected to scenario analysis with alternation of the following parameters: Unit cell size, unit cell shape, slit-thickness and thickness of the AS design as stated before.

The width of the structures must be taken into account. The clamps of the tensile machine are 4cm wide each, meaning that either the samples must be 4 cm wide each or the clamp length must be extended. Otherwise the sample is not uniformly elongated and the deformation behaviour is impossible to study accurately (see figure 35 in appendix).

The solution chosen for this is making the samples just as wide as the clamps, thus 4 cm. The size of the samples does not matter as long as the total size among the samples remain the same and the strain also remains the same for each experiment. Furthermore, this solution is chose for time efficiency also. The manufacturing process will be sped up drastically due to the fact that the 3D printed does have to cover a substantially smaller area.

A. Samples

To perform the scenario analysis on this AS model, different samples need to be created with different parameters. The thickness of the sheets in the initial 3D prints were 0.5mm. Buckling out of the plane occurred

however on these samples when a strain of 10% was applied.

There are two solutions to this problem. First, apply less strain on the sample. The second solution is to make the samples stronger in the plane the strain is applied on. The second solution was chosen, since the applied strain of 10% is needed for the observation of the deformation behaviour under tensile testing. If the samples are too thin, the AS structure is not strong enough to maintain the deformation within its plane. If the samples are thick enough the structure will be held in plane while performing tensile testing on the samples. The thickness of the sheets of all samples is therefore 1.5mm to prevent the buckling effect.

The first sample which is the base sample has the same scale metrics as the sample shown in figure 15. This sample structure has unit cells measuring 20mm by 20mm. It includes slits that are 0.6 times the length of the unit cell, making them 12mm long. Furthermore, the width of the slits is 1mm. In order to comply to the total structure width maximum of 4 cm, the unit cells are arrayed into two columns and four rows.

In the subsequent sample, parity with the baseline sample is maintained, except for a singular modification in the width of the slits, which is now set at 2mm. The unit cell dimensions remain consistent at 20mm by 20mm, and the length of the slits remains at 12mm.

In the final sample, the unit cell dimensions are reduced, with each unit cell now measuring 10mm as opposed to the initial 20mm. The slits maintain a consistent proportionality, still corresponding to 0.6 times the unit cell length, resulting in a slit length of 6mm. Additionally, the width of the slits experiences a reduction by half, now measuring 0.5mm. In order to maintain equivalence with the dimensions of the baseline sample, a twofold increase in the number of unit cells is implemented both horizontally and vertically. This adjustment ensures the preservation of the overall structure size while accommodating the altered unit cell scales. The parameters of each sample are shown in table I in the appendix.

The strain applied to these samples is 10%. The results of the simulations on these three samples can be seen in fig. 17, fig. 18 and fig. 19.

B. Poisson's ratio

The Poisson's ratio can be determined in COMSOL of all different samples. The displacement of the deformed samples are measured in COMSOL. The displacement is measured on the second unit cell row in the base and bigger slits samples and in the fourth unit cell row in the 0.5 scale unit cell size sample.

For the base sample the displacement is -1.1318mm and 1.1174mm. The total transversal displacement is then 2.25.

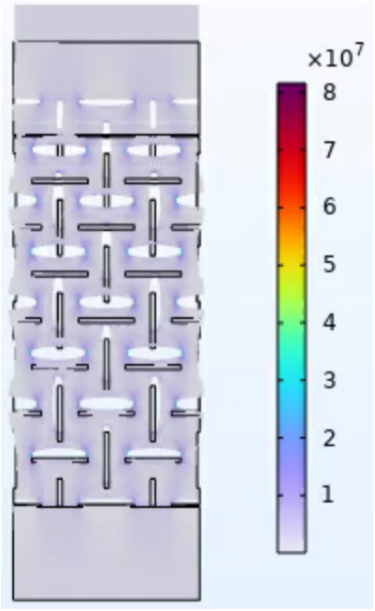

Fig. 17: AS base sample deformation behaviour under a 10% strain.

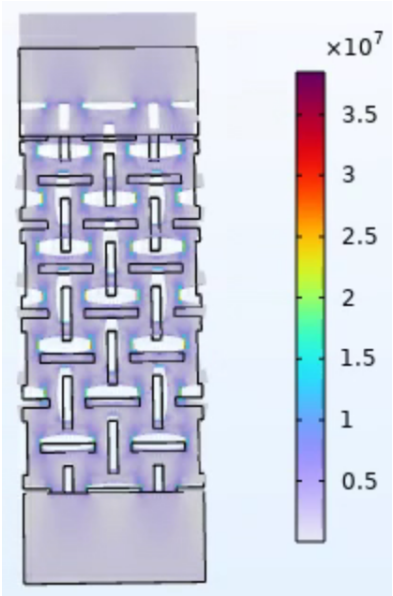

Fig. 18: AS with larger slits thickness 2mm sample deformation behaviour under 10% strain.

This means that the Poisson's ratio is

$$v = -\frac{2.25}{8} = -0.28 \tag{10}$$

For the bigger slits sample the displacement is -1.2722mm and 1.2737mm. The total transversal displacement is then 2.55mm. This means that the Poisson's ratio is

$$v = -\frac{2.55}{8} = -0.32 \tag{11}$$

For the 0.5 scale unit cell size sample, the measured displacement is -1.0934mm and 1.0590mm. The total transver-

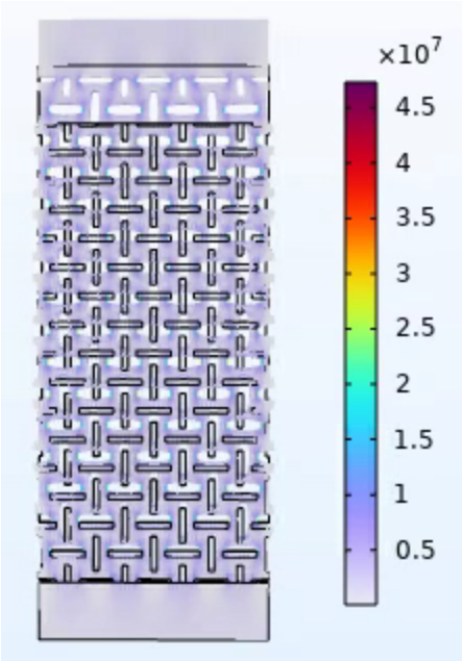

Fig. 19: AS with unit cell size scale 0.5 of base sample deformation behaviour under 10% strain.

sal displacement is then 2.15mm. This means that the Poisson's ratio is

$$v = -\frac{2.15}{8} = -0.27 \tag{12}$$

The Poisson's ratio is the highest for the sample with the bigger slits in the COMSOL simulated environment. Furthermore, the maximum stress exerted on the structure is in this sample is lower than the base and the 0.5 scale unit cell size sample.

C. Elastic modulus

The elastic modulus (stiffness) of the structure is calculated by the stress over strain. This equation is given in equation 13.

$$E = \frac{\sigma}{\varepsilon} \tag{13}$$

where

$$\sigma = \frac{F}{A} \qquad \varepsilon = \frac{u}{l} \tag{14}$$

E is the stiffness of the structure in N/m^2. F is the reaction force generated on the structure for the prescribed displacement in N and A is the area in m^2 on which the force is acted upon. u is the prescribed displacement in mm and l is the original length of the structure in mm. Combining equations 13 and 14 gives the following equation for stiffness [28]

$$E = \frac{F * l}{A * u} \tag{15}$$

The elastic modulus of each sample can also be computed by evaluation the reaction forces each sample generated when a certain strain is applied. The strain applied is 10%, which is in each case 8mm. The reaction forces of the base sample, the sample with bigger slits and the sample with unit cell sizes of scale 0.5 are 122.45N, 98.087N and 107.48N respectively. u is 8mm for all samples, since the prescribed displacement is set to 8mm. l is 80 mm for all samples, since all samples have the original length of 80 mm. A is also the same in all samples namely 60mm^2. The length of this block is 40mm (2 unit cells of 20mm or 4 of 10mm), and the width is 1.5mm (sheet thickness). This amounts to a elastic modulus for the base sample of

$$E = \frac{122.45 * 80}{60 * 8} = 20.41\text{N/mm}^2 \tag{16}$$

The elastic modulus of the sample with bigger slits amounts to

$$E = \frac{98.087 * 80}{60 * 8} = 16.35\text{N/mm}^2 \tag{17}$$

The elastic modulus of the sample with a 0.5 scale unit cell size amounts to

$$E = \frac{107.48 * 80}{60 * 8} = 17.91\text{N/mm}^2 \tag{18}$$

X. TENSILE STRENGTH TESTING

The experimental setup is as follows, the 3D printed structure design is clamped by two clamps of a tensile strength machine. The bottom clamp is fixed, while the top clamp moves up causing the structure to undergo tensile displacement. The deformation behaviour filmed with a camera so that it can be analysed. Additional data is acquired by the program, which include total force needed for displacement, total displacement of the top clamp and total time elapsed.

The following samples are fabricated to conduct the tensile strength testing and observing the deformation behaviour. These samples can be seen in figure 20.

The tensile test results are visualised in fig. 21, fig. 22 and fig. 23. The begin position of each sample under a 0% strain is shown and the end position under 10% strain is shown.

The Poisson's ratio of each sample is determined using an open-source software ImageJ. The transversal displacement and axial displacement is measured by measuring the displacement of the pixels. The transversal displacement of the base sample, bigger slits sample and 0.5 scale unit cell size sample are 27 pixels, 24 pixels and 15 pixels respectively. The axial displacement of the base sample, bigger slits sample and 0.5 scale unit cell size sample are 78 pixels, 78 pixels and 75 pixels respectively. The Poisson's ratio for each sample is then calculated as displayed the equation below where the equation on the left is for the base sample, the

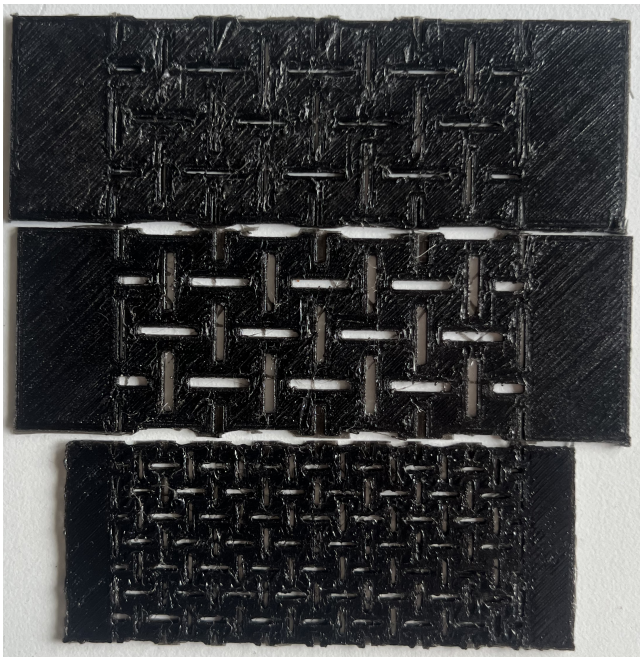

Fig. 20: Samples of the AS design; The top sample is the base sample; The middle sample is the sample with bigger slits; The bottom sample is the sample with 0.5 scale unit cells. *Nota bene*: the gripping part of the bottom sample are also of scale 0.5. This does not influence the tensile testing, as the clamps will only hold on to the gripping parts. This just means that not the whole area of the clamps is in contact to the gripping parts of this sample.

equation in the middle for the bigger slits sample and the equation on the right for the 0.5 scale unit cell size sample.

$$v = -\frac{27}{78} = -0.35 \quad v = -\frac{24}{78} = -0.31 \quad v = -\frac{15}{75} = -0.20 \tag{19}$$

The results of the tensile testing experiments can be summarized in a force over displacement graph. These graphs are displayed in figure 37. The ramp of these graphs determine the order of the elastic modulus of the structure. The ramp that corresponds to each graph is determined using excel. The ramp of the base sample, bigger slits sample and unit cell size of scale 0.5 samples are 8.2387, 6.6376 and 4.9838 respectively. The elastic modulus is computed with the data acquired from the tensile testing. The total reaction force generated at a 10% strain is 82.7429N for the base sample, 55.8541N for the sample with bigger slits and 47.2051N for the sample with a 0.5 scale unit cell size. This results in an elastic modulus of 13.79N/mm^2 for the base sample,

$$E = \frac{82.7429 * 80}{60 * 8} = 13.79\text{N/mm}^2 \tag{20}$$

9.31N/mm^2 for the sample with bigger slits and

$$E = \frac{55.8541 * 80}{60 * 8} = 9.31\text{N/mm}^2 \tag{21}$$

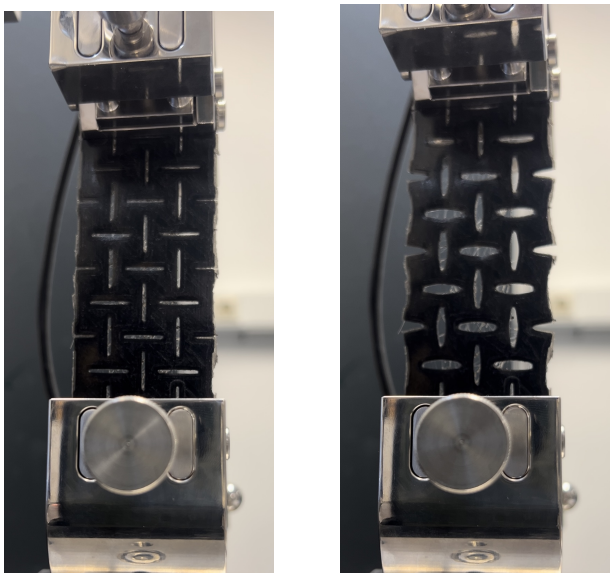

(a) Begin position (b) Ending position

Fig. 21: Begin position and end position of the base sample at tensile testing.

an elastic modulus of 7.87N/mm^2 for the sample with 0.5 scale for unit cell size.

$$E = \frac{47.2015 * 80}{60 * 8} = 7.87\text{N/mm}^2 \tag{22}$$

XI. VALIDATION OF COMSOL SIMULATIONS BY TENSILE TESTING

A. Poisson's ratio

The COMSOL simulations show that the bigger slits sample has the lowest Poisson's ratio (-0.32), the sample with 0.5 scale unit cell size has the highest Poisson's ratio (-0.27) and the base sample is in between (-0.28).

The tensile testing shows that the base sample has the lowest Poisson's ratio (-0.35), the sample with 0.5 scale unit cell size has the highest Poisson's ratio (-0.20) and the sample with bigger slits is in between (-0.31).

The magnitude of the Poisson's ratio for the bigger slits sample is the same. The difference of 0.01 is negligible, therefore the simulation is verified. The difference in the other two samples can however not be neglected. These differences are influence by several factors such as the precision of the measurement in the software used and the setup of the tensile testing. The difference in order of the Poisson's ratio magnitude is most likely also caused by imprecise setup of the tensile testing.

B. Elastic modulus

The COMSOL simulations show that the base sample has the largest elastic modulus (20.41N/mm^2), the bigger slits sample has the smallest elastic modulus (16.35N/mm^2)

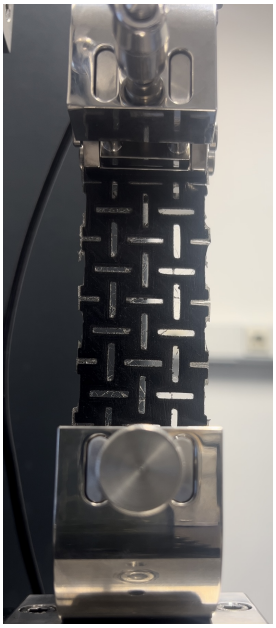

(a) Begin position

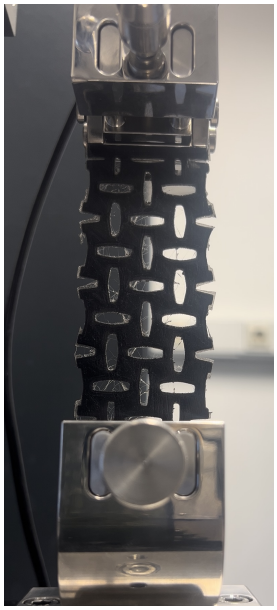

(b) End position

Fig. 22: Begin and end position of bigger slits sample.

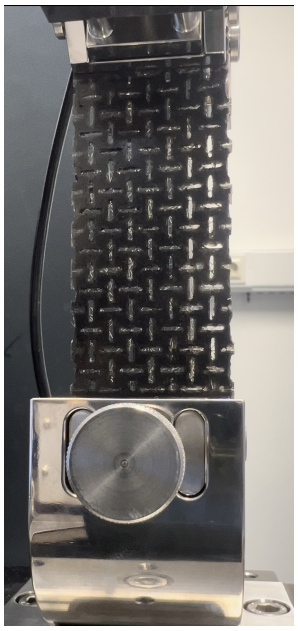

(a) Begin position

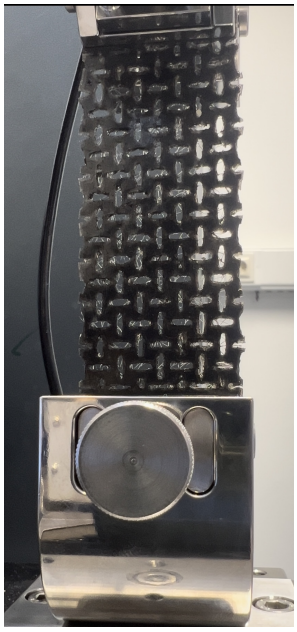

(b) End position

Fig. 23: Begin and end position of 0.5 scale unit cell size sample.

and the sample with a 0.5 scale unit cell size has a elastic modulus in between (17.91N/mm^2).

The tensile testing shows that the base sample has the largest elastic modulus (13.79N/mm^2), the sample with 0.5 scale unit cell size has the smallest elastic modulus (7.87N/mm^2) and the sample with bigger slits has a elastic modulus (9.31N/mm^2) in between.

The differences in the order of elastic modulus computed of the three samples by the COMSOL simulations and tensile testing is most likely causes by faultiness in the set up of the experiments. The initial position of the top clamp of the tensile machine is extremely important for the force values that are acquired. If in the initial position of the experiment the top clamp is too high and the structure is already stretched, the force that will be needed for a 8mm strain is too high. Consequently, if the initial position of the top clamp is too low, the force that is needed for a 8mm strain will be too low.

The differences in the magnitude of the elastic modulus can be explained by this same fact. The initial position of the top clamp was not high enough, this means that the overall force needed for a displacement of 8mm of the top clamp.

Another reason for the differences in the computed values for the Poisson's ratio and elastic modulus are the imperfections and or quality of the prints. Additionally, the support of the prints needed to be cut out by hand. This means that the cut outs are not of the same quality as the COMSOL models and that there will be different quality across the samples. The latter is however expected to have little to no effect in the obtained results.

XII. CONCLUSION DISCUSSION AND FURTHER WORK

The best metamaterial structure for the shoulder strap design of a passive exoskeleton that will be worn by ambulance personnel and nurses to alleviate spinal load during work is the Alternating Slit (AS) design. This AS design is auxetic and offers extraordinary stability. Furthermore, the deformation behaviour is stable and distributed well across the design. This AS design serves the purpose of this application the best among the studied auxetic structures.

The parameter analysis shows that for an increase in slit thickness the elastic modulus of the structure decreases. Thus for a larger slit thickness the amount of force required for a 10% strain is lower. In the COMSOL simulation is shown that for an increase in slit thickness the maximum exerted stress on the structure decreases.

Scaling down the unit cell size also results in a lower elastic modulus for the structure. Thus for a scaled down unit cell size, the amount of force required for a 10% strain is less. Furthermore, the maximum stress exerted on the structure decreases with a scaled down unit cell size.

The Poisson's ratio increases for the sample with 0.5 scale unit cell size. The relationship between the Poisson's ratio and the thickness of the slits is however not clear. The COMSOL simulation show that the Poisson's ratio decreases

when the thickness of the slits increase, while the tensile testing contradicts this. To conclude on the relationship between the thickness of the slits and the Poisson's ratio further research needs to be conducted.

The tensile testing setup is extremely important to gather all correct data. The top clamp of the tensile machine was not in perfect state. The attachment which needed to ensure that the clamp was directly above the bottom clamp was not functioning 100%. There was no way to ensure that the top clamp was directly perfectly and not in a twisted position above the bottom clamp.

For the tensile testing setup there was also no precise method used to ensure that the initial position of the top clamp was perfect. This probably caused as already discussed for incorrect data, especially the force needed to displace the top clamp by 8mm.

There was also no use of a digital image correlation (DIC) system. Instead, only a camera was available for video frames. This resulted in using an open-source software ImageJ to measure the transversal and axial displacement of the begin frame and end frame. The calculated Poisson's ratio is therefore less reliable compared to using a DIC system.

A suggestion for further work is to research the best suited exact dimensions of the parameters of the AS design for the application of shoulder straps in a passive exoskeleton. Moreover, the current proposed design is optimised for 3D printing manufacturing available at the RUG. This means that the slits needed to be rectangular and minimum of 0.5mm thick, otherwise due to the nozzle of the Ultimaker 3 it would not be able to make an adequate print of the structure. Accordingly the best suited design of the slits should be researched upon (E.G. smaller slit thickness, more like incisions or slits ending in one point or in a semi-circle rather than rectangular).

XIII. ACKNOWLEDGEMENT

The author of this report would like to thank dr. Anastasiia Krushynska and PhD student Zhaohang Zhang for the incredible guidance and help, especially the day to day supervision and guidance by Zhaohang.

REFERENCES

[1] Y. He, D. Eguren, T. P. Luu, and J. L. Contreras-Vidal, "Risk management and regulations for lower limb medical exoskeletons: A review," *Medical Devices: Evidence and Research*, vol. Volume 10, pp. 89–107, 2017.

[2] C. Van Weel, H. Schers, and A. Timmermans, "Health care in the netherlands," *The Journal of the American Board of Family Medicine*, vol. 25, no. Suppl 1, S12–S17, 2012.

[3] T. B. Christoph Aluttis and M. W. Frank, "The workforce for health in a globalized context – global shortages and international migration," *Global Health Action*, vol. 7, no. 1, p. 23 611, 2014, PMID: 28672439. eprint: https://doi.org/10.3402/gha.v7.23611.

[4] X. C. Tong, "Concepts from metamaterials to functional metadevices," in *Functional Metamaterials and Metadevices*. Cham: Springer International Publishing, 2018, pp. 1–21.

[5] X. Ren, R. Das, P. Tran, T. D. Ngo, and Y. M. Xie, "Auxetic metamaterials and structures: A review," *Smart Materials and Structures*, vol. 27, no. 2, p. 023 001, 2018.

[6] M. Mir, M. N. Ali, J. Sami, and U. Ansari, "Review of mechanics and applications of auxetic structures," *Advances in Materials Science and Engineering*, vol. 2014, pp. 1–17, 2014.

[7] J. N. Grima and R. Gatt, "Perforated sheets exhibiting negative poisson's ratios," *Advanced Engineering Materials*, vol. 12, no. 6, pp. 460–464, 2010.

[8] E. Shojaei Barjuei, D. Caldwell, and J. Ortiz, "Bond graph modeling and kalman filter observer design for an industrial back-support exoskeleton," *Designs*, vol. 4, Dec. 2020.

[9] G. N. Greaves, A. L. Greer, R. S. Lakes, and T. Rouxel, "Poisson's ratio and modern materials," *Nature Materials*, vol. 10, no. 11, pp. 823–837, 2011.

[10] J. U. Surjadi, L. Gao, H. Du, *et al.*, "Mechanical metamaterials and their engineering applications," *Advanced Engineering Materials*, vol. 21, no. 3, p. 1 800 864, 2019.

[11] Y. Wang, J. Qiu, H. Cheng, and X. Zheng, "Analysis of human–exoskeleton system interaction for ergonomic design," *Human Factors: The Journal of the Human Factors and Ergonomics Society*, vol. 65, no. 5, pp. 909–922, 2020.

[12] N. Annamalai, S. Kamaruddin, I. Abdul Azid, and T. Yeoh, "Importance of problem statement in solving industry problems," *Applied Mechanics and Materials*, vol. 421, pp. 857–863, 2013.

[13] F. Ackermann and C. Eden, "Strategic management of stakeholders: Theory and practice," *Long Range Planning*, vol. 44, no. 3, pp. 179–196, 2011.

[14] P. Verschuren and H. Doorewaard, *Designing a research project*. Eleven International Publishing, 2010.

[15] A. A. Zadpoor, "Mechanical meta-materials," *Materials Horizons*, vol. 3, no. 5, pp. 371–381, 2016.

[16] G. W. Milton and A. V. Cherkaev, "Which elasticity tensors are realizable?," 1995.

[17] M. Kadic, T. Bückmann, N. Stenger, M. Thiel, and M. Wegener, "On the practicability of pentamode mechanical metamaterials," *Applied Physics Letters*, vol. 100, no. 19, 2012.

[18] T. Bückmann, R. Schittny, M. Thiel, M. Kadic, G. W. Milton, and M. Wegener, "On three-dimensional dila-

tional elastic metamaterials," *New journal of physics*, vol. 16, no. 3, p. 033 032, 2014.

[19] R. O. Ritchie, "The conflicts between strength and toughness," *Nature materials*, vol. 10, no. 11, pp. 817–822, 2011.

[20] F. Barthelat and R. Rabiei, "Toughness amplification in natural composites," *Journal of the Mechanics and Physics of Solids*, vol. 59, no. 4, pp. 829–840, 2011.

[21] X. Li, W. Peng, W. Wu, J. Xiong, and Y. Lu, "Auxetic mechanical metamaterials: From soft to stiff," *International Journal of Extreme Manufacturing*, vol. 5, no. 4, p. 042 003, 2023.

[22] S. Wang, C. Deng, O. Ojo, B. Akinrinlola, J. Kozub, and N. Wu, "Design and modeling of a novel three dimensional auxetic reentrant honeycomb structure for energy absorption," *Composite Structures*, vol. 280, p. 114 882, 2022.

[23] R. Krulwich, *What is it about bees and hexagons?* May 2013.

[24] C. Thieulin, C. Pailler-Mattéi, M. Djaghloul, A. Abdouni, R. Vargiolu, and H. Zahouani, "Wear of the stratum corneum resulting from repeated friction with tissues," *Wear*, pp. 259–265, 2017.

[25] V. Gupta, G. Singh, and A. Chanda, "Development of novel hierarchical designs for skin graft simulants with high expansion potential," *Biomedical Physics & Engineering Express*, vol. 9, no. 3, p. 035 024, 2023.

[26] C. L. Caristan, *Laser cutting guide for manufacturing*. Society of manufacturing engineers, 2004.

[27] B. Budiansky, "Theory of buckling and post-buckling behavior of elastic structures," *Advances in applied mechanics*, vol. 14, pp. 1–65, 1974.

[28] J. D. Lord and R. Morrell, "Elastic modulus measurement—obtaining reliable data from the tensile test," *Metrologia*, vol. 47, no. 2, S41, 2010.

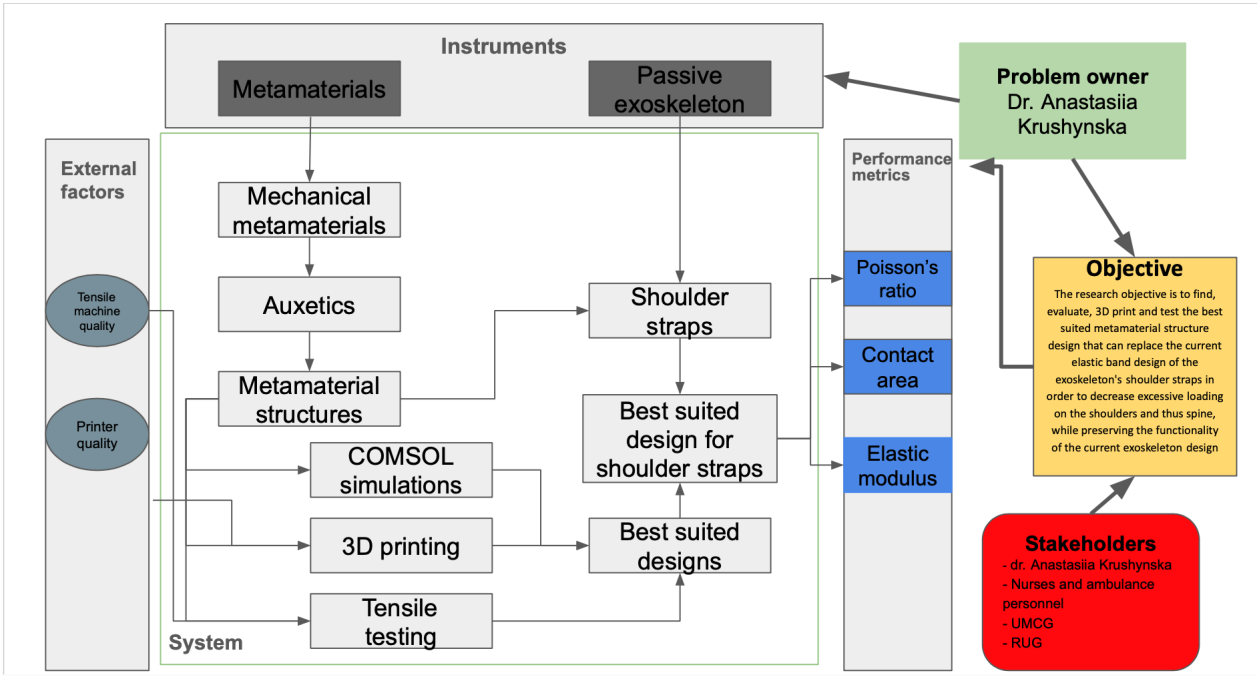

Fig. 24: Visualisation of system description.

XIV. APPENDIX

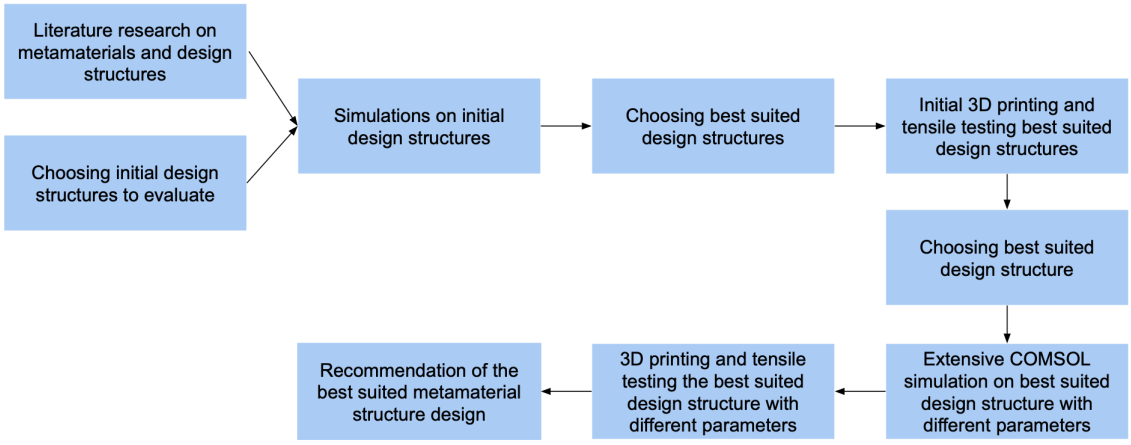

Fig. 25: Research framework.

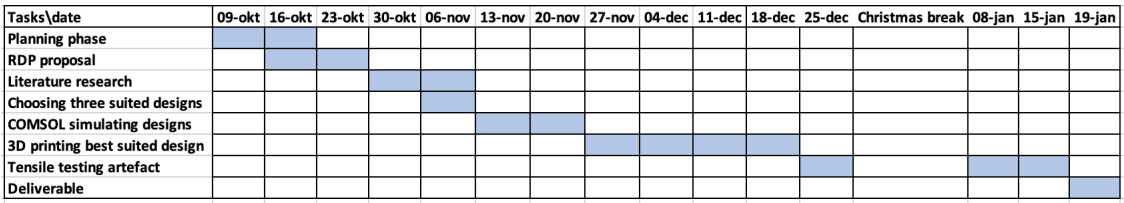

Fig. 26: Gantt chart of the research planning.

Sample/Parameters	Slit Thickness	Unit Cell Size	Sheet thickness	Slit length	Formed Array
Base	1mm	20mm x 20mm	1.5mm	12mm	2x4
Big Slits	2mm	20mm x 20mm	1.5mm	12mm	2x4
0.5 Scale Unit Cell Size	0.5mm	10mm x 10mm	1.5mm	6mm	4x8

TABLE I: Table with overview of parameters of each sample.

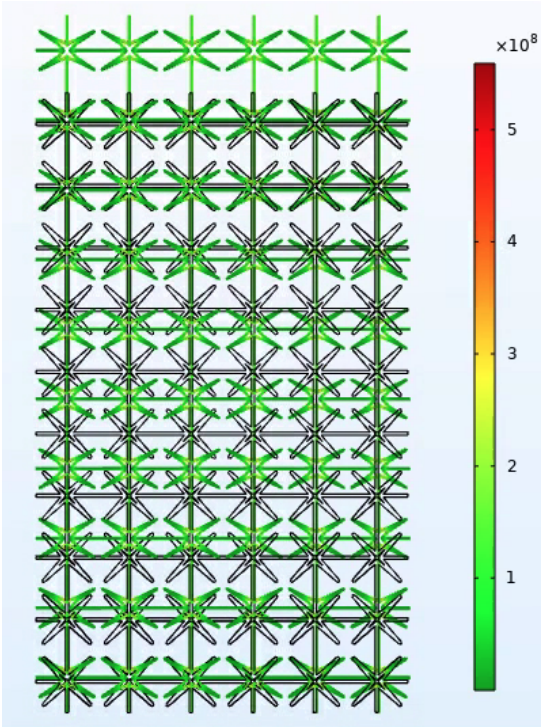

(a) Smaller angle θ

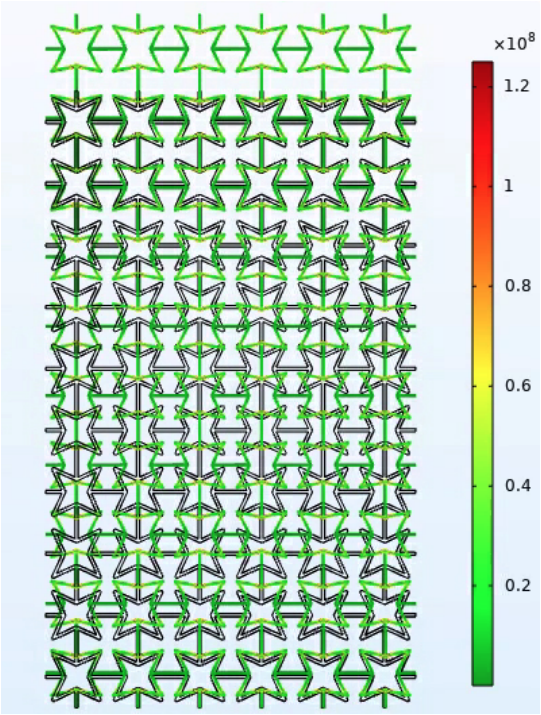

(b) Bigger angle θ

Fig. 27: Deformation behaviour of re-entrant star shaped design with smaller and bigger angle θ.

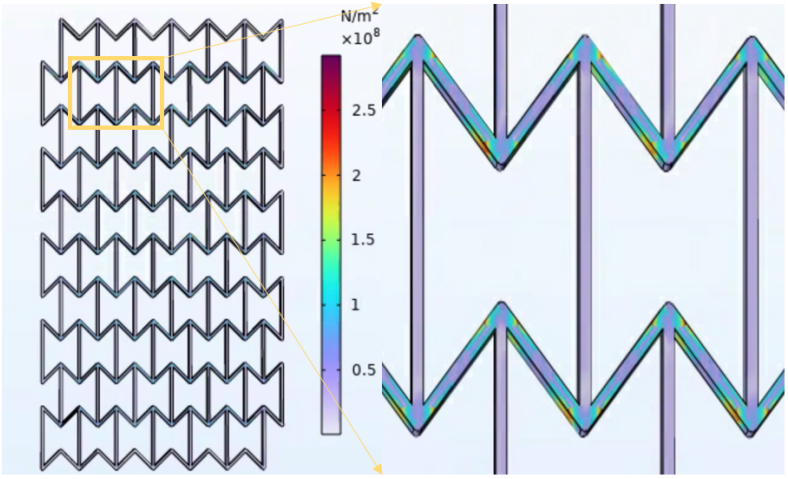

Fig. 28: The von Mises stress acted upon the non-deformed structure and a close up of this structure with the von Mises stress (N/m^2).

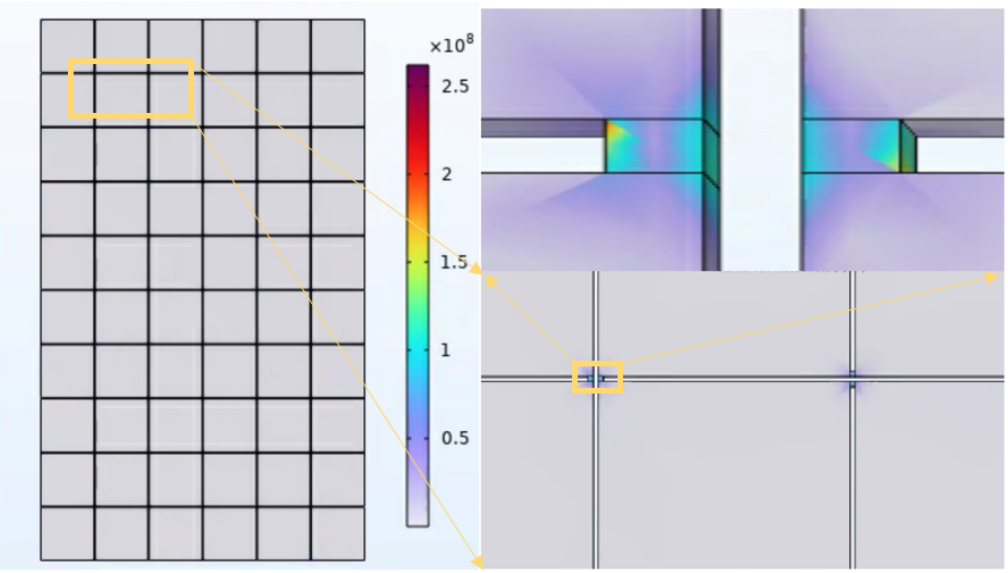

Fig. 29: The von Mises stress acted upon the non-deformed structure and a close up of this structure with the von Mises stress (N/m^2).

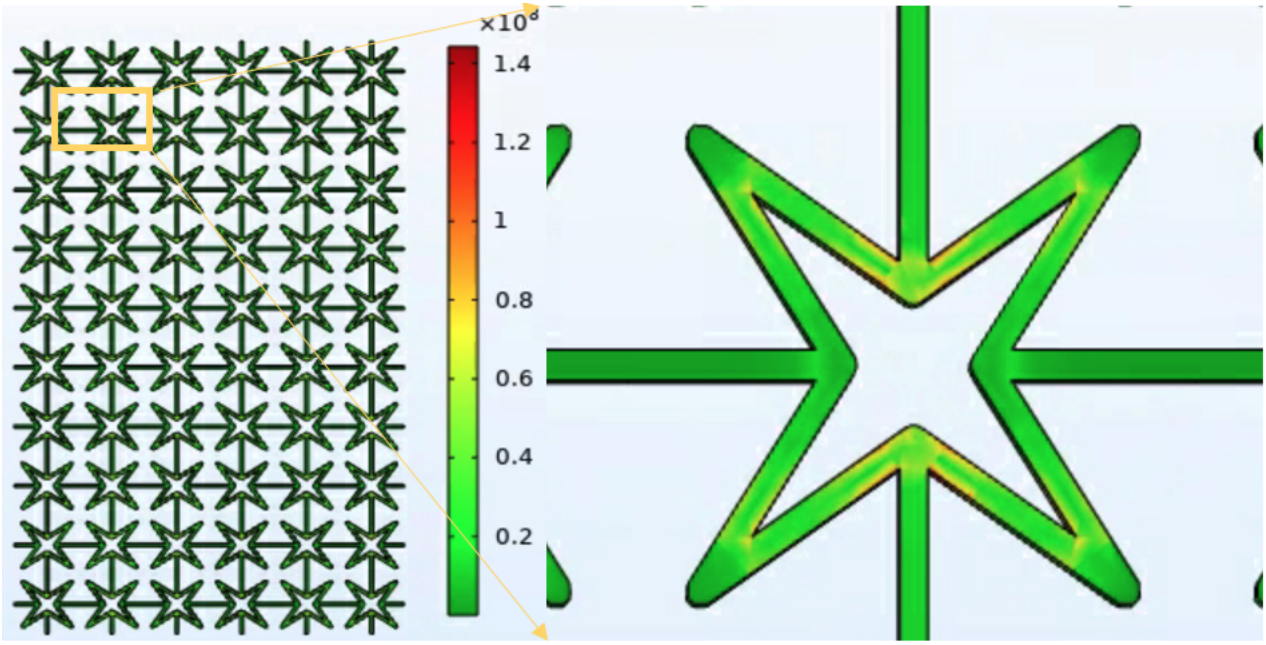

Fig. 30: The von Mises stress acted upon the non-deformed structure and a close up of this structure with the von Mises stress (N/m^2).

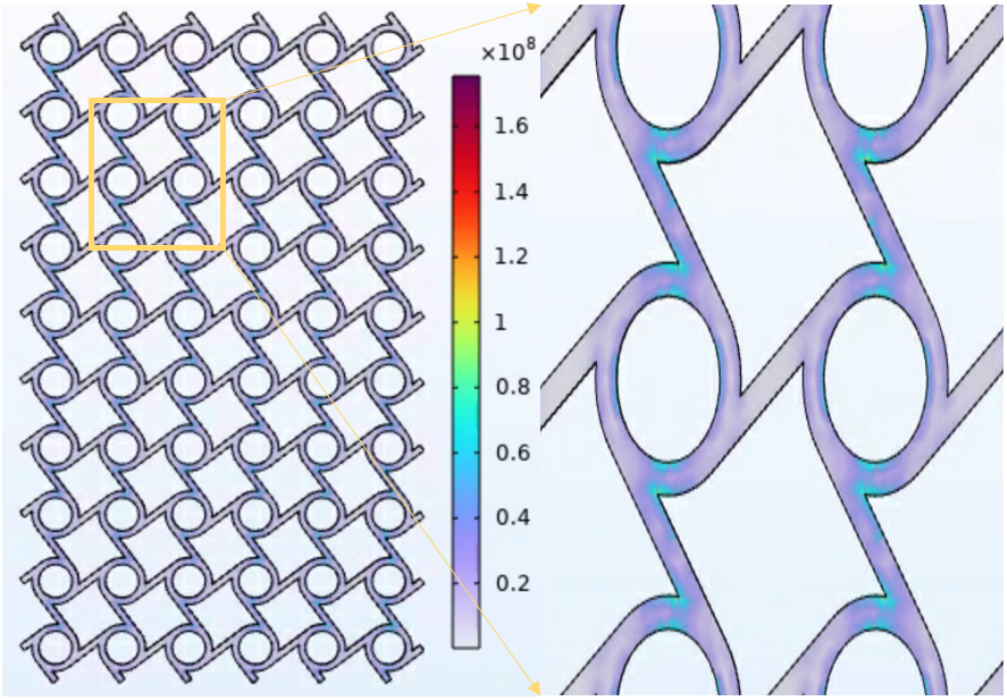

Fig. 31: The von Mises stress acted upon the non-deformed structure and a close up of this structure with the von Mises stress (N/m^2).

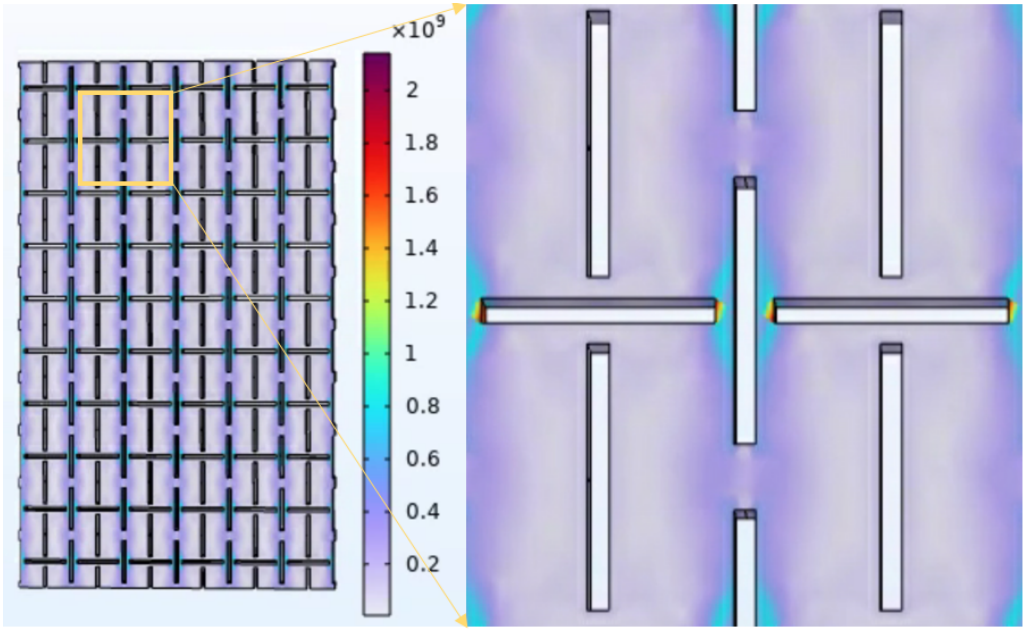

Fig. 32: The von Mises stress acted upon the non-deformed structure and a close up of this structure with the von Mises stress (N/m^2).

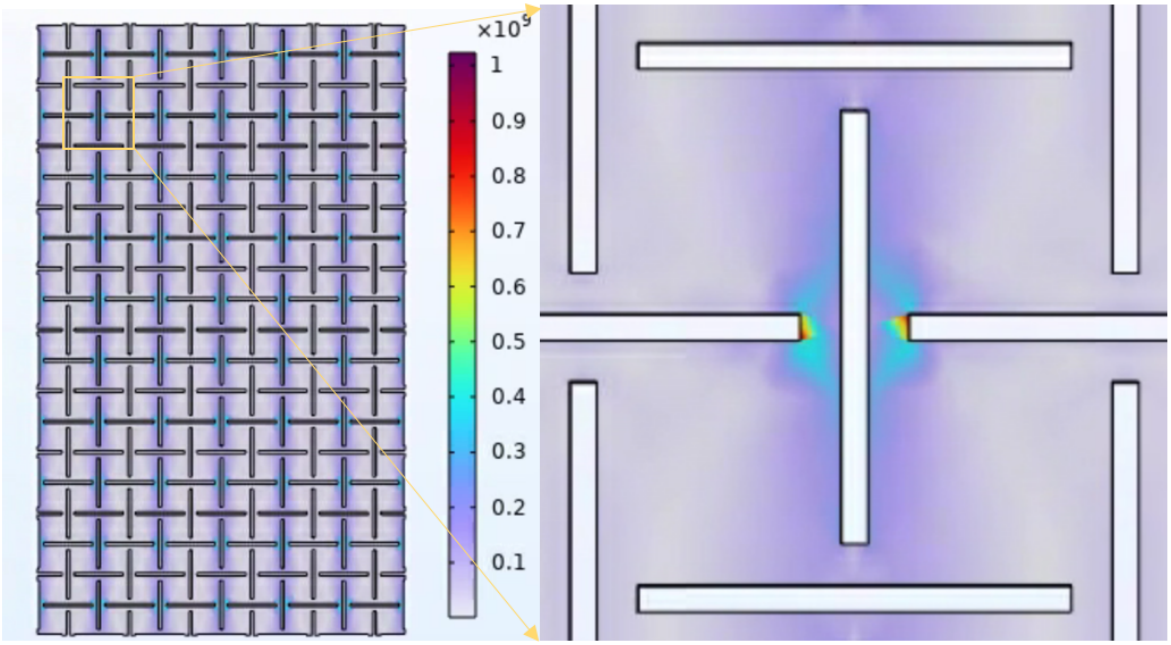

Fig. 33: The von Mises stress acted upon the non-deformed structure and a close up of this structure with the von Mises stress (N/m^2).

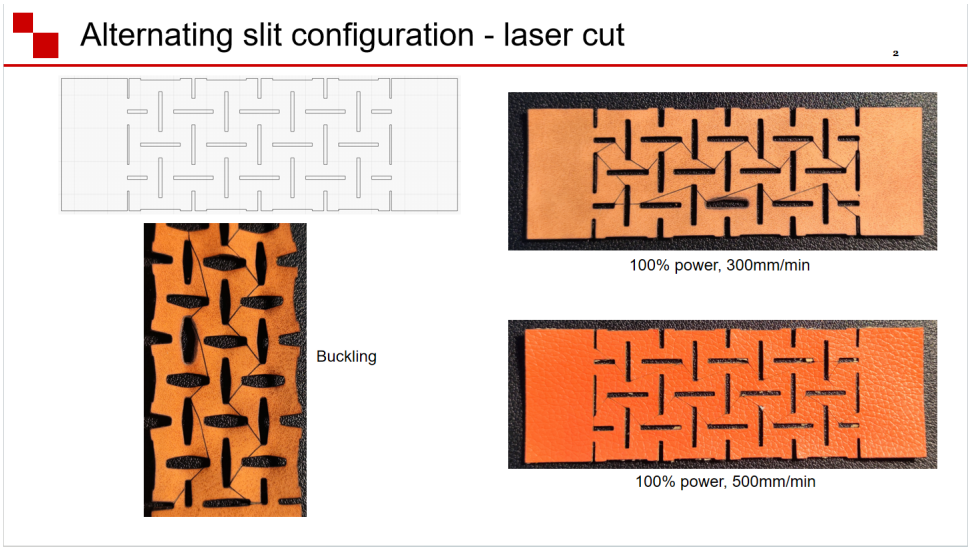

Fig. 34: Laser cutting technique on AS model. Adopted form PhD student Zhaohang Zhang.

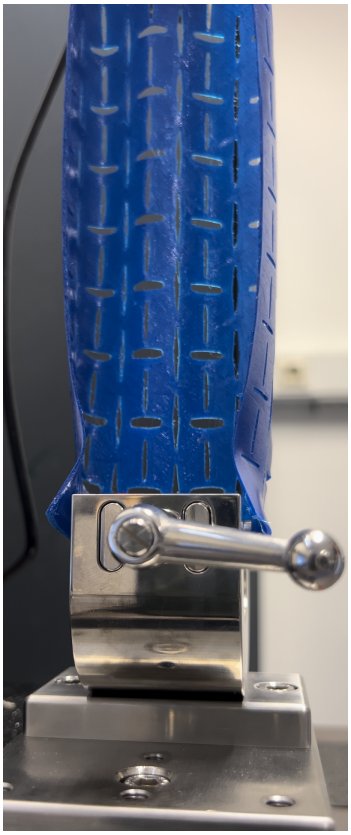

Fig. 35: Deformation of AS design where the width is too large, causing the design to not deform uniformly.

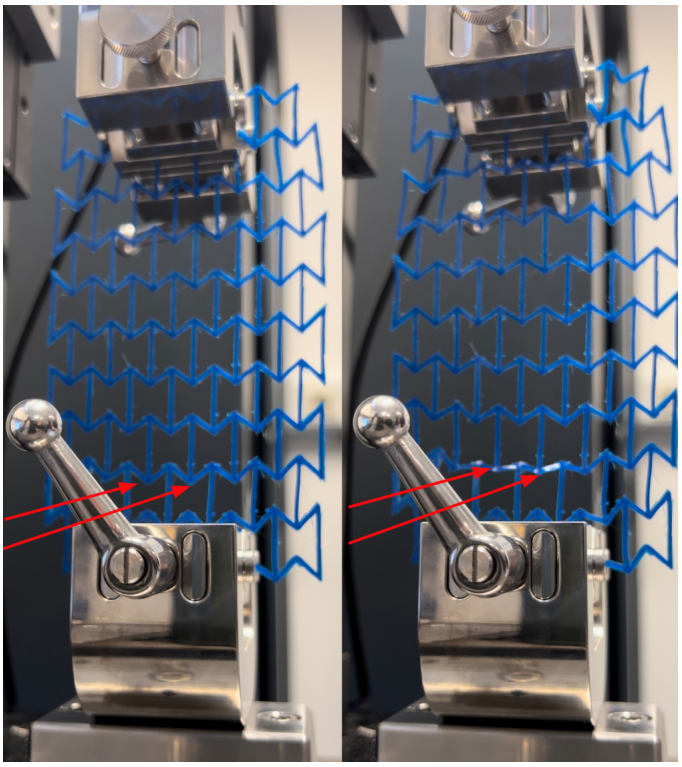

Fig. 36: Buckling effect on the honeycomb design. The red arrows show two places where buckling occurs on the honeycomb design under tensile loading.

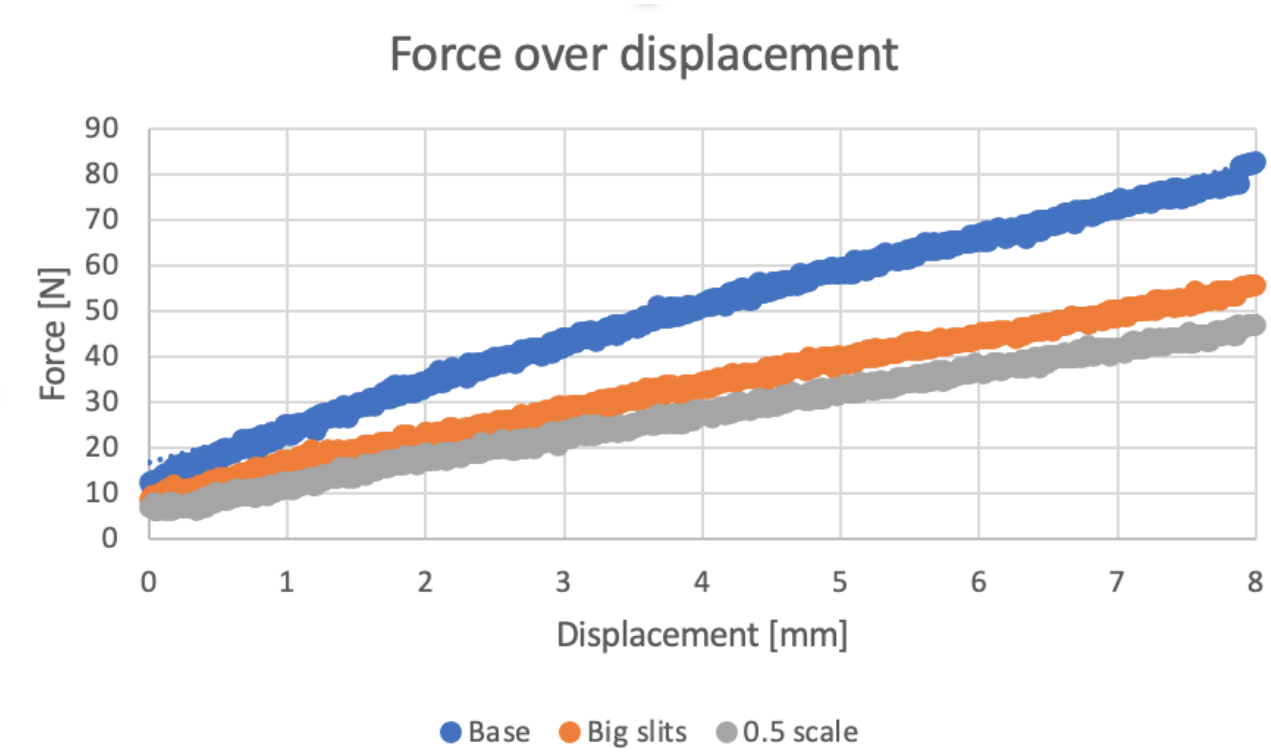

Fig. 37: Force over displacement graphs of all different samples.